Study of radiation background at the north crossing point of the BEPC Ⅱ in collision mode*

MO Xiao-Hu(莫晓虎)[1;1)] ZHANG Jian-Yong(张建勇)[1] ZHANG Qing-Jiang(张清江)[1]
Achasov Mikhail[2] CAI Xiao(蔡啸)[1] FU Cheng-Dong(傅成栋)[1] Harris Fred[3]
LIU Qian(刘倩)[3] Muchnoi Nikolay[2] QIN Qing(秦庆)[1] QU Hua-Min(屈化民)[1]
WANG Yi-Fang(王贻芳)[1] XU Jin-Qiang(徐金强)[1] ZHANG Tian-Bao(张天保)[1]

[1] Institute of High Energy Physics, Chinese Academy of Sciences, Beijing 100049, China
[2] Budker Institute of Nuclear Physics, Novosibirsk 630090, Russia
[3] Hawaii University, 12345, USA

Abstract: Understanding the radiation background at the north crossing point (NCP) in the tunnel of BEPCII is crucial for the performance safety of the High Purity Germanium (HPGe) detector, and in turn of great significance for long-term stable running of the energy measurement system. Therefore, as the first step, a NaI(Tl) detector is constructed to continuously measure the radiation level of photons as background for future experiments. Furthermore, gamma and neutron dosimeters are utilized to explore the radiation distribution in the vicinity of the NCP where the HPGe detector will be located. Synthesizing all obtained information, the shielding for neutron irradiation is studied based on model-dependent theoretical analysis.

Key words: radiation dose, shielding thickness, photon and neutron background, NaI(Tl) detector

PACS: 07.89.+b, 28.41.Qb, 29.40.Wk **DOI:** 10.1088/1674-1137/35/7/009

1 Introduction

A high-accuracy beam energy measurement system is being constructed at BEPC Ⅱ that is of great importance for the forthcoming physics analyses at BESⅢ, such as τ mass measurement, charmonium resonance scans, and determination of the branching ratio with uncertainty at the level of 1%–2% [1]. The whole system is determined to be allocated at the north crossing point (NCP) of the BEPC Ⅱ storage ring [2, 3], as shown in Fig. 1 and Fig. 2 of Ref. [4]. Here, the Compton backscattering (CBS) technique is utilized to measure the beam energy with fairly high accuracy [5]. The special concern for BEPC Ⅱ lies in the fact that the High Purity Germanium (HPGe) detector has to be located near the vacuum tubes of the electron and positron beams in the storage ring tunnel. Such a situation is very different from other systems, where the HPGe detector is usually protected by a radiation shielding wall [6, 7]. Because of the continuous immersion in the radiation field, the germanium crystals are subjected to a flux of photons and neutrons. The latter is a formidable killer for the HPGe detector since the irradiation by fast neutrons induces lattice defects inside the germanium crystals that act as charge carrier trappers and thus degrade the energy resolution of the detector seriously [8].

Besides the safety considerations for the HPGe, the radiological-safety protection for workers is another important factor for radiation dose measurement. For the BEPC Ⅱ experiment, there is merely one shielding concrete wall with a thickness of 0.5 meters between the tunnel and the corridor for the optics system, where some adjustments and inspection work should be performed when the machine is in operation. With all of this in mind, we must know as much as possible about the irradiation distribution

Received 15 September 2010, Revised 8 November 2010

* Supported by National Natural Science Foundation of China (10491303, 10775412, 10825524), Instrument Developing Project of Chinese Academy of Sciences (YZ200713), Major State Basic Research Development Program (2009CB825200, 2009CB825203, 2009CB825206) and Knowledge Innovation Project of Chinese Academy of Sciences (KJCX2-YW-N29)

1) E-mail: moxh@mail.ihep.ac.cn

at the NCP. Therefore, the preliminary measurements of radiation dose were performed from February to March in 2008, and some results were obtained, according to which it has been determined that moderate protection is enough to guarantee the proper working of the HPGe detector [4].

However, further measurements are necessary due to many factors. Firstly, most of the preliminary measurements were performed under the synchrotron mode, which is rather different from the real data-taking mode (collision mode). Therefore, more experiments are needed to proceed under the collision mode. Secondly, more experimental points are needed to acquire comparatively accurate distributions of radiation. Thirdly, the detection accuracy of neutrons should be improved to clear up the puzzle previously observed [4]. Lastly, more information can enhance the reliability of estimation for radiological-safety protection. Therefore, more meticulous measurements were performed. Consequently, the newly accurate data not only display considerable enhancement of the radiation backgrounds under the collision mode but also necessitate the special protection for the HPGe detector. The aim of this paper is to extend our understanding of the irradiation background by incorporating more information and to evaluate the shielding thickness for attenuating neutron irradiation on the grounds of theoretical analysis.

2 Measurement of the γ-spectra with a NaI(Tl) detector

The preliminary idea for constructing a NaI(Tl) detector is as follows. The HPGe detector is an expensive and highly sensitive instrument, and such a detector has never been located at the NCP of BEPC Ⅱ for the measurement of γ- and/or X-rays energy spectra. In order to acquire the practical conditions for HPGe, a NaI(Tl) detector is used, which is similar to an ordinary HPGe detector in detection efficiency of γ/X-rays.

As a matter of fact, the following experiments (refer to section 3) really indicate that the HPGe detector cannot be located at the NCP directly without any radiation protection.

2.1 Experimental setup

The γ-spectra detection system can be divided into three parts (refer to Fig. 1 for a block diagram of the system):

1) NaI(Tl) detector, whose function is to collect radiation photons;

2) signal-to-digital conversion system, which includes one NIM (nuclear instrument module) crate and one MCA (multichannel analyzer);

3) two computers, one for signal processing and the other for further data analysis.

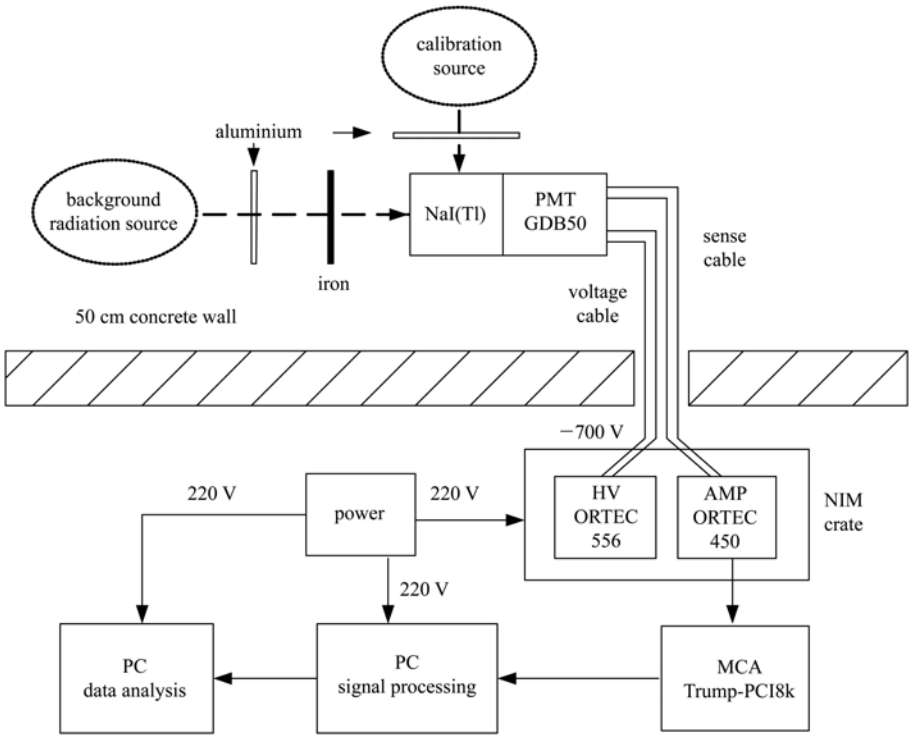

Fig. 1. Block diagram of γ-spectra detection system. The background sources exist when BECP Ⅱ is in the running state while the calibration source is used only when BECP Ⅱ stops running.

The large NaI ingots can be grown from high-purity sodium iodide to which a 10^{-3} mole fraction of thallium has been added as an activator [9]. As a hygroscopic material, NaI(Tl) is wrapped with aluminium foil to avoid deterioration. The wrapped cylindrical crystal (ϕ45 mm×40 mm) is coupled immediately with photomultiplier GDB50, all of which is put in a magnetic shielding cylinder (ϕ7 cm×23.6 cm with a wall thickness of 2 mm) made of soft iron, and encapsulated in an aluminum box (10 cm×10 cm×32 cm with a wall thickness of 2 mm).

The NaI(Tl) detector (refer to Fig. 2 for its construction) is connected to the NIM crate by a 50-meter-long radio-frequency cable (SEYV-100-3) and a 35-meter-long high voltage cable (SYV-75-5, uplimit of voltage is at the level of 5000 V). The signal pulse from the photomultiplier is transformed to the amplifier ORTEC450, and in turn transformed to a 8192 MCA, where an analog-to-digital converter (ADC) is used to convert each pulse into a channel number, so that each channel corresponds to a narrow range of pulse heights. As pulses arrive over time, the MCA collects in memory a distribution of the number of pulses with respect to the pulse height. This distribution, arranged in the order of ascending energies, is referred to as a spectrum.

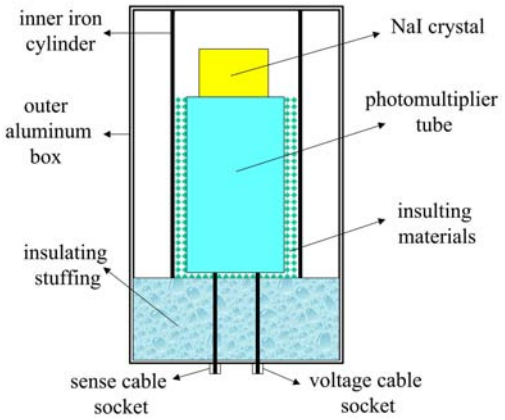

Fig. 2. Sketch configuration of NaI(Tl) detector. NaI(Tl) crystal (ϕ45 mm×40 mm) coupled with photomultiplier GDB50, put in a magnetic shielding cylinder (ϕ7 cm×23.6 cm with a wall thickness of 2 mm) made of soft iron, and encapsulated in an aluminum box (10 cm×10 cm×32 cm with a wall thickness of 2 mm).

Further data analysis is accomplished by MAESTRO software[1)], which is the vital link for the hardware of both the multichannel buffer (MCB) and the personal computer (PC). The MCB performs the actual pulse-height analysis, while the computer and operating system make available the display facility and data-archiving hardware and driver. Combined with the MCB and the PC, the MAESTRO software emulates a MCA with remarkable power and flexibility and shows continuously the spectrum being acquired. At the same time, the software provides all important operations that need to be performed, such as spectrum searching, locating, scaling, and report generating, printing and archiving, and so forth.

The saved data in the signal processing PC can be copied to the data analysis PC, where more detailed study can be carried out with the help of an analysis package, such as PAW [11].

2.2 Detector calibration

Calibrations are performed in the stopping interval of the accelerator running to acquire the relation between the ADC channels and gamma energy. During the stopping period, the ^{60}Co γ-ray source[2)] is just put on the top of the outer aluminium box (refer to Fig. 2). Then MAESTRO software [10] is utilized to perform the peak searching first. Here the Mariscotti method [12] is adopted.

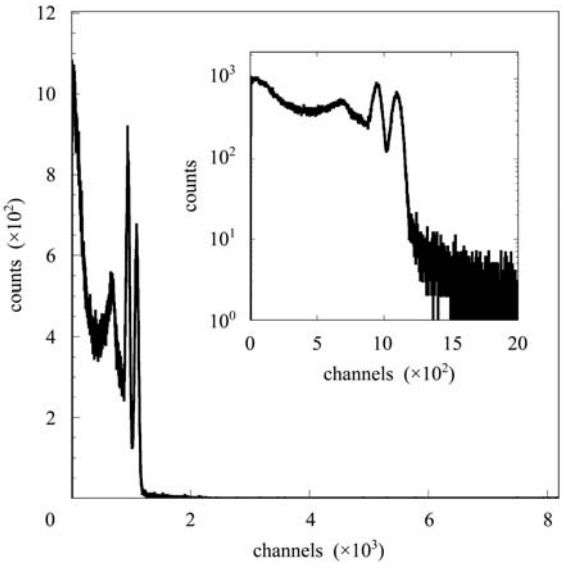

Fig. 3. Calibration results for ^{60}Co with two energy peaks at 1332.51 keV and 1173.23 keV, respectively.

When well-separated clean peaks are fixed, the calibration can be carried out by supplying the ener-

1) The software used in our experiments is MAESTRO-32 Version 6. The operation details can be found in the user's manual [10].

2) Besides a ^{60}Co γ-ray source, Pu-C source is also tried for calibration. Such a calibration attempt fails due to the weakness of the activity of the Pu-C source.

gies for these peaks. The calibration is stored with the spectrum and retained until the new calibration is performed.

During the experiment interruptions, a ^{60}Co source is used frequently to calibrate the detector avoiding the energy drift.

2.3 Result and discussion

Some results[1)] are exemplified in Fig. 4 and Table 1, where the results for previous measurements are also shown for comparison. The interesting information provided in Table 1 includes the total counts ($N_{\rm tot}$) for each case; the counts between energies of 2 MeV and 7 MeV (N_{2-7}), which correspond to the designed beam energies ($E_{\rm beam}$) of BEPC Ⅱ ranging from 1 GeV to 2 GeV; the counts with energy below 2 MeV ($N_{<2}$); in addition, the counts at an energy of 5.64 MeV ($N_{5.64}$), which corresponds to the τ mass energy ($E_{\rm beam}$=1.777 GeV).

Next we analyze the information and data in Fig. 4 and Table 1. Generally speaking, the results of the first, second, and third measurements are similar, and these are rather different from the previous measurements. Firstly, it can be seen for all four measurements that the $N_{\rm tot}$ are marginally at the same level of order of magnitude (10^8), and this is also true for $N_{<2}$. From the ratio of $N_{<2}/N_{\rm tot}$, it can be seen that more than 70% of the photon background is at energies of less than 2 MeV, which is beneficial for future beam measurement.

Secondly, it is obvious that N_{2-7} of this year measurement is much different from that for last year.

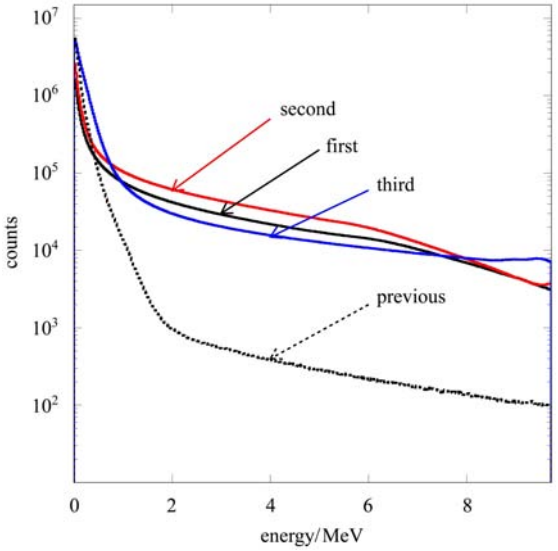

Fig. 4. Data recorded by NaI(Tl) detector at the NCP for first, second, and third time measurement. The bin-width of the abscissa is around 1.185 MeV. For comparison, the results from the previous measurements are also presented.

This year's results are 40 to 80 times greater than those of a year earlier. The great difference is reasonabe due to the different running mode. That is to say, the radiation level at the collision mode will be greater than that at the synchrotron mode.

Thirdly, for the photon background with energy at 5.64 MeV, the number of largest counts amounts to 0.24 per second, which is considerably smaller than the expected HPGe detector rate, which is at the level of 10^4 per second [5].

Table 1. Results from the NaI(Tl) detector corresponding to the first, second, third, and previous measurements. (The results of previous measurements are given in Ref. [4]. The meaning of 1st, 2nd and 3rd measurement refers to Section 3, and the position of the NaI(Tl) detector is at ①, as indicated in Fig. 5 with coordinate (0, 379, 115)). Int.Curr. indicates integral current while A·H is for Ampere times Hour. The meaning of listed variables here can be found in the text.

	first	second	third	previous
date/yy.mm.dd	2009.2.20	2009.3.12	2009.5.18	2008.3.8
Int.Curr./A·H				
($\mathcal{I}_{e+}+\mathcal{I}_{e-}$)	5.50 + 2.82	6.85 + 8.13	7.92 + 6.26	0 + 4.58
$N_{\rm tot}$/day	3.84×10^8	5.53×10^8	9.76×10^8	5.75×10^8
$N_{\rm tot}$/sec.	4.45×10^3	6.41×10^3	1.13×10^4	6.66×10^3
N_{2-7}/day	8.82×10^7	1.29×10^8	6.43×10^7	1.58×10^6
N_{2-7}/sec.	1020	1494	744.1	18.34
$N_{<2}$/day	2.83×10^8	4.10×10^8	8.93×10^8	5.71×10^8
$N_{5.64}$/day	1.50×10^4	2.11×10^4	1.13×10^4	228

1) The experiment runs from February to July of 2009. The measurement results are recorded automatically in a series of files and the time-length for each file is three hours (before May 18th, 2009) or one and half minutes (after May 18th, 2009). All files are surveyed and a few of them are selected that reflect the comparatively stable running state of BEPC Ⅱ. At the same time, the time-interval is selected to be consistent with the period of dosimeter measurement.

3 Dose measurements by dosimeter

3.1 Landauer's service

There are two types of probe that are extensively used for radiation dose measurement. The first one is the optically stimulated luminescence detector (OSLD) made of carbon-doped aluminum oxide (Al_2O_3: C) which is mainly used for γ, β and X-ray detection; the second is the solid state nuclear track detector (SSNTD) made of allyl diglycol carbonate ($C_{12}H_{18}O_7$), shortened to CR-39, which is mainly used for neutron detection. The working principles of these two detectors, which can be found in Refs. [13, 14], are briefly introduced in Ref. [4], and described in great length in books [15, 16].

The radiation dosimeters used at BEPC II are provided by Landauer® Incorporated Company [17].

Landauer grows the special formulated $Al_2O_3:C$ crystalline detector material, which is then often configured into a laminated disk sandwiched between two mylars. So far as CR-39 is concerned, it is usually made into a small square. Used in this work is an IZ-type dosimeter, which actually consists of both I-type and Z-type dosimeters. The former is built on an assembly of a case component with a metal and plastic filter along with a four-positioned OSLD slide component; while the latter is composed of one SSNTD and a ploye thylene radiator. The energies detected by OSLD range from 5 keV to 40 MeV for γ and X-ray while those detected by SSNTD range from 40 keV to 40 MeV for fast neutrons. The corresponding doses measured are from 0.01 mSv to 10 Sv (γ and X-ray), 0.1 mSv to 10 Sv (β), and 0.2 mSv to 250 mSv (neutron), respectively.

All components of the IZ-type dosimeter are installed in the Landauer holder, which usually has an alligator clip for secure fastening to clothing [17]. Anyway, for experiments at IHEP, the dosimeters are mainly used to measure the environmental dose, therefore holders are put on supports or fixed to the wall with adhesive tape.

When the measurement is finished, all dosimeters are collected and returned to Landauer for analysis. The Al_2O_3:C detector is read out by the OSL technique. The reader stimulates the probes with a light emitting diode array, causing it to luminesce in proportion to the amount of radiation exposure. The luminescence is detected and measured by the reader's photo multiplier tube using a high sensitivity photon counting system. A dose calculation algorithm is then applied to the measurement to determine the exposure results. For neutron analysis, the CR-39 is etched for 15 hours in a chemical bath to enlarge the exposure tracks. The fast neutron dose is measured by counting the tracks generated as a result of the proton recoil with the polyetheylene radiator. Within two or three weeks, the measurement results, as summarized in Table 2, are fed back from the Landauer company to IHEP by registration post.

3.2 Measurement design

Unlike the NaI(Tl) detector, which could provide continuous monitoring for the gamma background, the dosimeters are mainly used to acquire the gamma and neutron spatial distributions, and they must be placed in the cubic space of the NCP. Since each time a total of twenty IZ-type dosimeters are provided by Landauer, and one has to be left to record the dose of the nature background, only nineteen dosimeters are available for dose measurement. In order to obtain as much information as possible under such conditions, the detailed measurement plan is made to take into account many factors, as described below.

Firstly, the dose distribution of the horizontal plane of the beam pipe (HPBP) is of paramount importance for the shielding design. Therefore, a total of twenty-two points are measured in this plane (refer to Fig. 5 for the special positions of these points, and all of them with the z-axis value 120 cm, see Table 2). Since we expect that the radiation level due to positrons is greater than that of electrons, more points are allotted on the east side (where the positrons circulate within the inner ring) than on the west side. This is the reason why the distribution of points is asymmetric with respect to the y-axis.

Secondly, when the laser beam collides with the electron/positron beam, the backscattering photons will be detected by the HPGe. So the straight line of backscattering photons (LBP) that is to pass through the HPGe is another important region where the radiation should be understood in detail. Then seven points are arranged along this line, as shown in Fig. 5 (from west to east, the seven points are respectively, ⑨, ④, ①, ②, ⑥, ⑦, and ⑧).

Thirdly, since the cubic distribution of radiation level is to be measured, many points are arranged in the vertical direction at positions ①, ②, ⑥, and ⑩, as denoted by the dots with circles in Fig. 5.

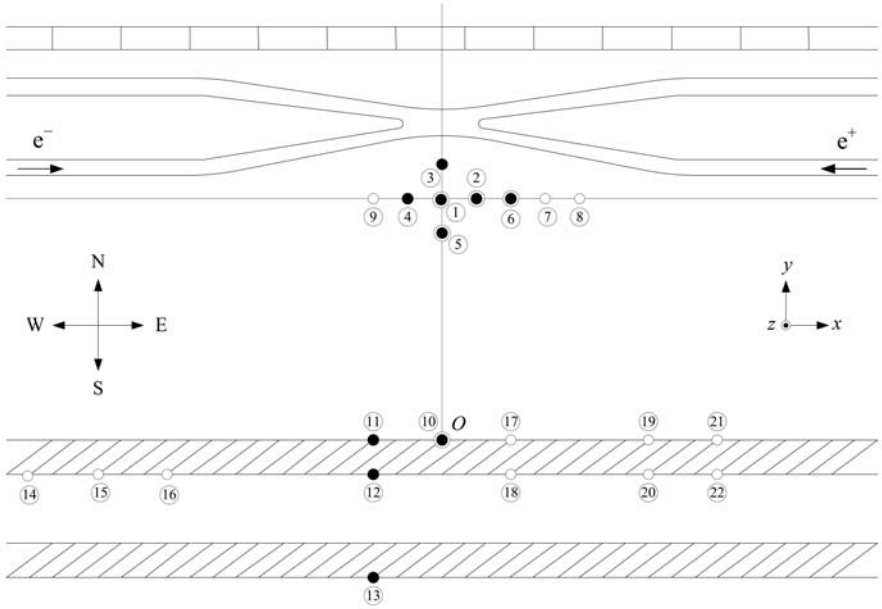

Fig. 5. Schematic view of dosimeter distributions at the NCP of BEPC Ⅱ. The "O" denotes the origin of coordinates that does not coincide with the NCP. The positive (negative) x-axis represents the east (west) direction; the positive (negative) y-axis represents the north (south) direction; $z = 0$ denotes the ground level of the storage ring tunnel; and the positive (negative) z-axis represents the upwards (downwards) direction. Two hatched bands indicate the two concrete walls with thickness 50 cm each; the top block band denotes the support for machine wires and cables; and the two bands crossed at the NCP delineate the vacuum pipes for the electron and positron beams. The blank circles indicate only one measurement performed here; the black dots indicate more than one measurement performed here; the dots with circles indicate that more than one dosimeter is located at the position with the same x and y coordinates but a different z coordinate, and more than one measurement are performed.

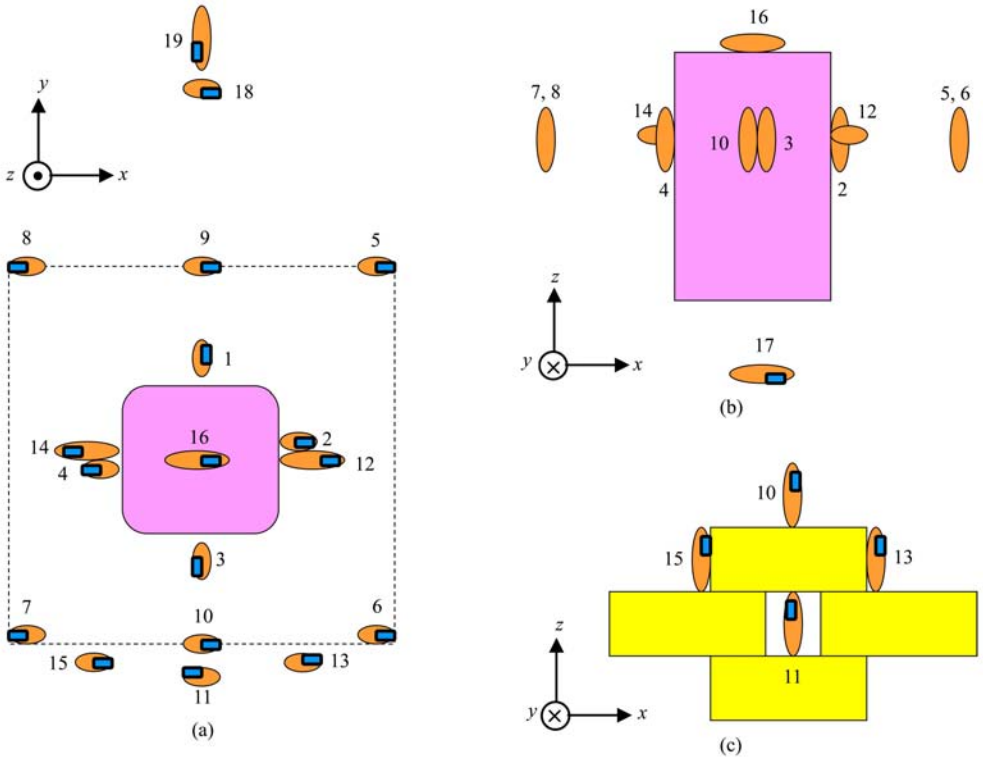

Fig. 6. Schematic plot for dosimeter distribution of the fourth measurement. The coordinates definition is the same as that in Fig. 5. (a) The vertical view; (b) the side view (1); (c) the side view (2).

Table 2. Results of radiation dose measurement. The meanings of coordinates x, y, and z are the same as in Fig. 5. As reference and comparison, the dose limit [18] for an occupational work is 100 mSv in 5 years and at the same time the dose cannot be more than 50 mSv in any year.

serial number	position (x,y,z)/cm	measured dose/mSv					
		γ&X	neutron	γ&X	neutron	γ&X	neutron
		first time		second time		third time	
⓪	background	0.02	0.10	0.09	0.06	0.14	0.06
①	(0,370,120)	147.97	27.58	88.8	2.02	157.91	1.91
①a	(0,370,170)	76.03	1.04				
①b	(0,370,70)	73.09	1.52	79.15	0.96		
①c	(0,370,20)	28.47	1.29			21.77	1.39
②	(50,370,120)	81.97	1.18	76.49	1.45	81.49	1.85
②a	(50,370,170)			42.80	0.54		
②b	(50,370,70)	27.55	1.56	37.66	0.69		
②c	(50,370,20)			17.93	1.00		
③	(0,420,120)	792.07	2.20	341.98	19.49	497.93	14.71
④	$(-50,370,120)$	89.15	2.45	70.58	1.58	77.14	1.48
⑤	(0,320,120)	29.01	1.45	29.35	0.69	28.47	1.00
⑥	(100,370,120)	68.06	1.10	61.80	1.06	74.38	2.10
⑥a	(100,370,170)					61.69	1.00
⑥b	(100,370,70)					48.37	1.18
⑦	(150,370,120)			71.62	1.23	79.47	1.43
⑧	(200,370,120)					107.94	2.35
⑨	$(-100,370,120)$	84.41	1.56				
⑩	(0,0,120)	23.25	1.50	21.64	0.29	27.34	1.18
⑩a	(0,0,20)	16.74	1.02	15.17	0.58	19.17	0.85
⑪	$(-100,0,120)$	21.23	1.50	18.91	0.46	24.89	0.94
⑫	$(-100,-50,120)$	<0.02	<0.1	<0.02	<0.1	0.02	<0.1
⑬	$(-100,-220,120)$	<0.02	<0.1	<0.02	<0.1	<0.02	<0.1
⑭	$(-700,-50,120)$	<0.02	<0.1				
⑮	$(-600,-50,120)$			<0.02	<0.1		
⑯	$(-500,-50,120)$					<0.02	<0.1
⑰	(100,0,120)	20.02	0.69				
⑱	$(100,-50,120)$	<0.02	<0.1				
⑲	(300,0,120)			34.67	1.48		
⑳	$(300,-50,120)$			0.07	<0.1		
㉑	(400,0,120)					82.86	2.91
㉒	$(400,-50,120)$					0.04	<0.1

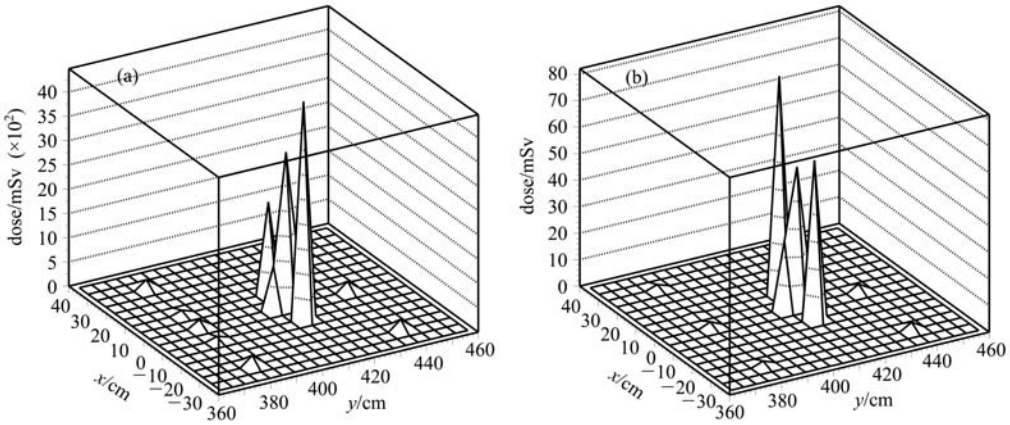

Fig. 7. Gamma and neutron radiation dose in the NCP for the fourth time measurement. The values of the following points are presented in the plot: from ① to ⑩, ⑬, ⑮, and ⑯. (a) The gamma radiation in the NCP; (b) the neutron radiation in the NCP.

Table 3. Results of radiation dose measurement at the position where the HPGe will be located. The fourth measurement was performed from June 16th to July 1st, 2009. The meanings of coordinates x, y, and z are the same as in Fig. 5. The second column presents the measured coordinates for each dosimeter. If two measured coordinates before and after each measurement are denoted as A and B, where A and B can be x, y, or z, then the numbers given in the table are represented by formula $(A+B)/2\pm|A-B|$.

serial number	position (x,y,z)/cm	measured value $(x\pm\delta x, y\pm\delta y, z\pm\delta z)$/cm	measured dose/mSv	
			γ&X	neutron
⓪	–		0.13	0.08
①	(0, 420, 120)	(0.0±0.0, 419.5±1.0, 117.8±1.5,)	917.03	13.04
②	(10, 415, 120)	(8.1±0.2, 412.5±1.0, 118.8±0.5,)	1883.23	82.00
⑫	(10, 415, 120)	(9.0±0.0, 410.0±0.0, 119.8±0.5,)	2441.80	54.94
③	(0, 410, 120)	(0.0±0.0, 403.5±1.0, 117.5±1.0,)	887.82	25.66
④	(−10, 415, 120)	(−8.5±0.0, 410.0±0.0, 119.0±0.0,)	4480.06	59.86
⑭	(−10, 415, 120)	(−9.0±0.0, 413.0±0.0, 120.0±0.0,)	3397.96	97.90
⑤	(30, 440, 120)	(28.0±2.0, 438.0±0.0, 120.2±0.5,)	237.44	2.16
⑥	(30, 380, 120)	(27.5±3.0, 384.0±0.0, 120.0±0.0,)	187.60	1.60
⑦	(−30, 380, 120)	(−26.8±2.5, 383.0±0.0, 119.5±1.0,)	209.33	1.63
⑧	(−30, 440, 120)	(−25.2±5.5, 439.8±0.5, 118.5±3.0,)	213.48	2.69
⑨	(0, 440, 120)	(0.5±1.0, 438.0±2.0, 116.0±2.0,)	203.09	2.69
⑩	(0, 380, 120)	(0.2±0.5, 383.5±3.0, 119.5±1.0,)	157.15	1.92
⑪	(0, 380, 110)	(0.0±0.0, 379.5±3.0, 100.5±9.0,)	48.43	0.35
⑬	(10, 380, 120)	(10.8±1.5, 381.5±1.0, 106.5±3.0,)	83.57	0.59
⑮	(−10, 380, 120)	(−9.5±1.0, 381.4±1.3, 107.0±2.0,)	68.38	0.37
⑯	(0, 415, 125)	(0.0±0.0, 411.5±1.0, 123.0±1.0,)	3177.26	52.54
⑰	(0, 412, 76)	(−0.5±1.0, 408.9±0.3, 76.0±0.0,)	7.63	1.76
⑱	(0, 485, 120)	(0.0±0.0, 486.5±0.0, 120.0±0.0,)	132.50	2.85
⑲	(0, 495, 125)	(0.0±0.0, 495.8±0.5, 124.5±1.0,)	539.29	4.08

Fourthly, because each time only nineteen dosimeters are available, the radiation levels at all planned positions are measured three times successively. In order to compare the distinctive doses measured in each time, and treat all measurement results as a whole, some points have to be measured each time, so that the dose measured at these points can be used to normalize the dose at other points, or at least these points could be used as the reference when the doses measured at different times are compared. A total of eleven points are measured each time, as denoted by the black dots in Fig. 5, or refer to Table 2.

After the three times' measurements, the general picture for the radiation background distributions in the vicinity of the NCP is obtained. As a further step study, the more detailed measurements around the point where the HPGe will be located are performed. Fig. 6 shows the schematic plot for the distributions of dosimeters in the fourth measurement. The coordinates of each point together with the measurement results are presented in Table 3.

3.3 Results survey

3.3.1 Radiation distribution

In the light of measurement results provided in both Table 2 and Table 3, the general feature of the radiation background distributions in the vicinity of the NCP can be understood. We begin with the neutron distribution:

1) By virtue of Table 2, except for a few points (① and ③), the neutron distribution is rather uniform, and the radiation dose in the tunnel is at least one order of magnitude greater than the reference background level. Behind the concrete protection wall, the radiation dose could be regarded as the same level as the reference background. This result also clears up the puzzle previously observed [4].

2) From Table 3 or more intuitively from Fig. 7, it is obvious that the radiation level along the line of backscattering photon (LBP) is 30 or 50 times greater than other positions.

As far as the photon distribution is concerned, it seems more complex than that of the neutron:

1) In the horizontal plan of the beam pipe (HPBP), the radiation level along the LBP is rather high. The corresponding radiation level decreases 20 or 30 times when it moves 25 to 30 cm away north- or southwards (along the positive or negative direction of the y-axis) from the LBP.

2) Unlike the uniform distribution of the neutron

in the tunnel, the radiation level decreases obviously when it moves away up- or downwards (along the positive or negative direction of the z-axis) from the HPBP.

3) Although the radiation dose of the photon is fairly low behind the concrete protection wall, the radiation dose is detectable at some points (say, points ⑳ and ㉒ in Table 2).

4) It also seems that the fluctuation in radiation dose due to photons is greater than that due to neutrons.

3.3.2 Data comparison

It is expected that for the stable running state, the radiation level should be proportional to the beam current. However, during the period of our measurements, the running states of BEPC Ⅱ vary so much, and the conditions of irradiation are so distinguished that any simplistic normalization on the basis of beam current is not applicable for the measured radiation data. Some running state information is collected to provide a certain qualitative understanding of radiation level in different measurements.

Firstly, it is noticeable, as shown in Table 4 and Table 2, although the integrated current of the third measurement is more than three times greater than that of the first time, the radiation levels of the two measurements are almost the same. The only similar situation for the first and third time measurements is that lots of times are used for the accelerator machine study.

Secondly, it is presumed that the radiation level is relevant to the beam status, such as injection, beam lost, mode changing and so forth. As denoted by A, B, C, D in Table 4, four types of number of beam status are described as follows[1)]:

1) A denotes the number of beam injections;

2) B denotes the number of supplementary injections of beam;

Table 4. The information for dosimeter measurements. The integral current (Int.Curr.) is the summation of beam current for each time with unity of Ampere · Hour (A·H) while the average current (Avg.Curr.) is the Int.Curr. over the total time (with unity hour) used for beam operation.

	first time	second time	third time
date/yy.mm.dd	from 2009.2.17 (12:00)	from 2009.3.10 (12:00)	from 2009.5.13 (12:00)
(o'clock)	to 2009.2.24 (8:00)	to 2009.3.17 (12:00)	to 2009.5.27 (8:00)
Int.Curr./A·H			
positron(e^+)	21.22	51.02	71.20
electron(e^-)	17.45	43.71	58.50
Avg.Curr./mA			
positron(e^+)	164.0	322.6	306.9
electron(e^-)	156.2	276.3	289.3
beam state			
e^+: A,B,C,D	39, 47, 51, 3	17, 61, 4, 0	119, 59, 39, 0
e^-: A,B,C,D	22, 13, 17, 3	13, 66, 3, 0	123, 48, 38, 1
working state	accelerator machine study	ψ' data taking	accelerator machine study, mode change, and data taking

3) C denotes the number of beam fluctuations;

4) D denotes the number of beams lost.

According to values of A, B, C, D, it can be seen that the status of the second time measurement is comparatively stable and the radiation level is correspondingly low. In fact, during the period of the second time measurement, the BEPC Ⅱ is running for ψ' data taking and the running is fairly smooth.

Last, some remarks. Due to numerous and meticulous factors in accelerator running, it is impractical to evaluate the beam lost analytically for the stable running, let alone for unstable running status. The only numerical estimation is based on the Monte Carlo simulation, which is sometimes semi-quantitatively reliable. Therefore, for the time being, we satisfy ourselves with qualitatively understanding the relation between beam status and radiation level.

4 Irradiation protection

Synthesizing the preceding results, the irradiation protection for the HPGe is studied. At the out-

1) The definition of different types of number is not very strict, especially for B and C. Both B and C could be zigzag shaped except for their amplitude size. Sometimes the shape of C is rather irregular, which is very easily distinguished from that of B; but sometimes the amplitude of B is not much greater than C. For this case, the count of the number is rather random.

set, a simplistic formula is derived for estimation of the shielding thickness. Then a model-dependent theoretical analysis is performed where more realistic effects and complex situations are taken into consideration. Finally, a brief review is given for Monte Carlo software, which can provide more reliable information for irradiation protection design.

4.1 Simplistic estimation

Neutron attenuation and absorption in a shielding material can be depicted by an exponential function based on absorber thickness x (unit: cm) and the neutron removal coefficient $\mu_{\rm r}$ (unit: $\rm cm^{-1}$), or [19]

$$\dot{D}(x)=\dot{D}_0\cdot B\cdot {\rm e}^{-\mu_{\rm r}\cdot x}\ , \tag{1}$$

where $\dot{D}(x)$ is the dose equivalent rate outside a shield of thickness x; and $\dot{D}_0\equiv\dot{D}(0)$ is the dose equivalent rate for neutron radiation. The buildup factor B is necessary to account for neutrons that are scattered back into the beam after they undergo an elastic or inelastic collision in the absorber. Buildup factors for neutrons are sparse. Roughly speaking, a neutron buildup factor of about 5 is appropriate for most estimations in which water or paraffin shields of 20 cm or more are used. In the actual situation of BEPC Ⅱ, paraffin is used as the shielding material, so $\mu_{\rm r}$= 0.118 $\rm cm^{-1}$ is used for the following estimation[1)].

As a matter of fact, according to Eq. (1), it is obtained immediately,

$$x=\frac{1}{\mu_{\rm r}}\cdot\ln\frac{\dot{D}_0\cdot B}{\dot{D}(x)}\ . \tag{2}$$

Here what we really care about is the thickness of shields that can prevent the HPGe detector from the damage of neutron radiation. The value of $\dot{D}_0$ can be evaluated from the radiation background measurement data listed in Table 3. The measured neutron doses in the fourth measurement at points ②, ⑫, ④, ⑭, and ⑥ are averaged to obtain the total dose accumulated during 15 beam days. Finally, we have

$$\dot{D}_0=4.63\ \ {\rm mSv/day}\ . \tag{3}$$

The value of $\dot{D}(x)$ represents the required dose equivalent rate limitation behind the certain shielding. The relevant information for evaluating $\dot{D}(x)$ includes the damage uplimit of neutron fluence [20]; the fluence-to-dose conversion factor for neutrons at 10 MeV [19]; and the total data taking time for five years[2)]. With all information as collected in Table 5, we get

$$\dot{D}(x)=\frac{D_{\rm up}\cdot F_{\rm f.d.}}{T_{\rm tot}}=0.21\ {\rm mSv/day}. \tag{4}$$

So according to the evaluations in Eqs. (3) and (4), and values of $\mu_{\rm r}$ and B in Table 5, the shielding thickness x is calculated to be 39.9 cm.

Table 5. The required information for calculating the $\dot{D}_0$ and x.

symbol	meaning	value	unit
$D_{\rm up}$	damage uplimit of neutron fluence	1×10^7	neutron $\rm cm^{-2}$
$F_{\rm f.d.}$	fluence-to-dose conversion factor for neutron at 10 MeV	6.8×10^{-2}	$\rm (mSv\cdot h^{-1})/\ (neutron\ cm^{-2}\cdot s^{-1})$
$T_{\rm tot}$	total data taking time for five years	7.776×10^7	s
$\mu_{\rm r}$	removal coefficient for paraffin	0.118	$\rm cm^{-1}$
B	buildup factor	5	–

4.2 Analytic estimation

The simplistic estimation is easy, useful, and important; it can provide us with the general concept for the thickness of radiation protection. Anyway, such an estimation is too simple to be used for practical radiation design. More detailed analysis indicates that the dose equivalent rate can be evaluated by the formula

$$\dot{D}(x)=\int_{E_{\rm c}}^{\infty}{\rm d}E\cdot S(E,x)\cdot F_{\rm f.d.}(E)\cdot B(E,x)\cdot{\rm e}^{-\eta(E,x)}\ . \tag{5}$$

Here, all factors are actually neutron-energy-dependent; but for a special situation, some factors or part of them can be treated as constants since the variation in these factor is rather small within a rather wide energy region of neutrons. Now we explain the

1) More precisely speaking, $\mu_{\rm r}$ is an energy dependent function. However, within certain neutron energy, say from 1 MeV to 10 MeV, as a rough estimation, the constant value is a good approximation. More information relevant to $\mu_{\rm r}$ can be found in the following section 6.1.

2) The total data taking time only denotes the running time used for BESⅢ physics data taking. It is estimated with the following assumption, six months (180 days) for each year.

factors in Eq. (5) one by one. Firstly, for multilayer protection materials,

$$\eta(E,x)=\mu_{\rm r}^{\rm H}(x-t)+\sum_{i=1}^{n}\mu_{\rm r}^{i}t_i\ \left(\text{with } t=\sum_{i=1}^{n}t_i\right), \quad (6)$$

where x denotes the total shielding thickness, and t the total shielding thickness except for hydrogen materials. $\mu_{\rm r}^{\rm H}$ and $\mu_{\rm r}^{i}$ represent the removal coefficients of hydrogen (H) and element i. For briefness, in the following estimation, we only consider two shielding materials: lead and paraffin; moreover, we only consider the case when the thickness of the two materials is the same. As to the calculation of $\mu_{\rm r}^{\rm H}$ and $\mu_{\rm r}^{i}$, more detailed information can be found in Section 6.1.

Secondly, for two shielding materials, lead and paraffin, with the same thickness, the buildup factor is calculated as follows

$$B(E,x)=1+\frac{E-E_{\rm c}}{E}\cdot(\mu_{\rm r}^{\rm H}+\mu_{\rm r}^{\rm Pb})\cdot x. \quad (7)$$

Notice, when $x=0$, $B(E,0)=1$. This fact will be used to calculate $\dot{D}_0$.

Thirdly, the fluence-to-dose conversion factor for neutrons, $F_{\rm f.d.}(E)$, at different energy is calculated by the empirical formula

$$F_{\rm f.d.}(E)=7.5052-2.7358\,Y+2.6750\,Y^2-1.0918\,Y^3 +0.13510\,Y^4\ (\text{with } Y=\ln E). \quad (8)$$

The formula is obtained by fitting the values provided in Table 14-5 in Ref. [19] for neutron energy from 0.l MeV to 100 MeV. In fact, the value of $F_{\rm f.d.}$ in the previous section is also taken from this Table.

Fourthly, for the fluence distribution function $S(E,x)$, it is usually expressed as follows, [21]

$$S(E,x)=S_{\rm p}\cdot\chi(E)\cdot\mathcal{G}(E,x), \quad (9)$$

where $S_{\rm p}$ is the neutron emission strength; $\chi(E)$ the energy spectrum; and $\mathcal{G}(E,x)$ a point-source dose kernel. For our case, it is treated as a constant[1)], that is $\mathcal{G}(E,x)=g_0$. Since it is rather difficult to get the analytic expression for the neutron spectrum, as a rough estimation, we test three cases, that is

$$\begin{aligned}&\chi_1=\delta(E_0)\ (E_0=10\text{ MeV})\ ;\\ &\chi_2=\Theta(E-E_1)-\Theta(E_2-E)\\ &\qquad(E_1=1\text{ MeV},\ E_2=20\text{ MeV})\ ;\\ &\chi_3=E{\rm e}^{-bE}\ (1/b=10\text{ MeV})\ .\end{aligned} \quad (10)$$

For the last function of the energy spectrum, the derivative operation indicates that χ_3 accesses to its maximum value at $E=1/b$.

To avoid the normalization problem, the relative dose equivalent rate is calculated, viz.

$$R_{\rm dose}\equiv\frac{\dot{D}(x)}{\dot{D}_0}, \quad (11)$$

with

$$\dot{D}_0\equiv\dot{D}(0)=\int_{E_{\rm c}}^{\infty}{\rm d}E\cdot S_{\rm p}\chi(E)g_0\cdot F_{\rm f.d.}(E). \quad (12)$$

Last but not least, the integral low- and up-limit in the actual calculation are taken as 0.04 MeV and 100 MeV, respectively. As a matter of fact, the integral is rather insensitive to these integral limits, as shown in Fig. 8.

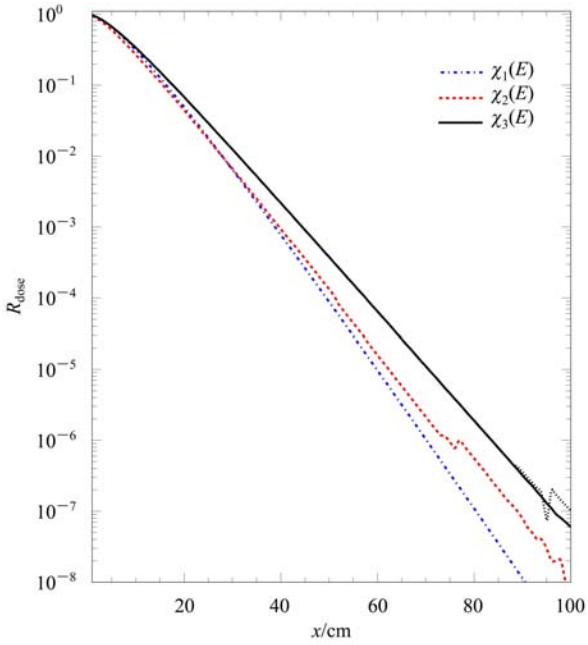

Fig. 8. Variation in dose equivalent rate against shielding thickness. The low- and up-limit of the integral are 0.04 MeV and 100 MeV, respectively. The black dotted line in the region from $x=90$ cm to 100 cm denotes the results for χ_3 spectrum but with the low- and up-limit of the integral being 0.01 MeV and 10000 MeV, respectively.

For the values obtained in Eqs.(3) and (4), $R_{\rm dose}\approx 0.05$, then from Fig. 8, $x\approx 20$ cm, which means the total shielding thickness is 40 cm with 20 cm lead and 20 cm paraffin. The evaluated value in this section coincides with that in the preceding section. Anyway, herein two materials instead of one are used for irradiation protection.

1) The Monte Carlo simulation indicates the distribution of dose near the NCP where the HPGe will be located, is almost uniform, that is position independent. As far as the energy dependent feature of $\mathcal{G}(E,x)$ is concerned, no experimental data are available and it is also assumed as a constant.

4.3 Simulation estimation

In Section 4.1, the simplistic estimation gives us an intuitive and qualitative concept for shielding thickness. In Section 4.2, the analytic estimation pedagogically exhibits the complex of radiation calculation. However, even the analytic estimation presented in this monograph is far from the accurate estimation. One of the annoying problems is that the attenuation of fast neutrons in a shield generally leads to neutrons with intermediate and, eventually, thermal energies. The latter, which are readily absorbed by the shield material, lead to the production of high-energy capture gamma-rays. This capture gamma-ray dose at the shield surface is usually an indispensable consideration in the shield design [21]. That is to say, in realistic estimation, both neutron and photon shielding should be considered simultaneously.

The precise and exact description of radiations and all of their interactions with shielding materials, often in complex geometries, is within the mandate of transport theory, which, in its turn, is a subdiscipline of statistical mechanics. The fundamental tool for solving the transport problem is the Boltzmann equation, which describes the behavior of the corpuscular ionizing radiation [22]. Nevertheless, because analytically solving the Boltzmann equation is extremely difficult, recourse to computational methods is usually necessary. The most frequently used computational techniques are in the light of the Monte Carlo approach, which is based on the use of random sampling to obtain the solution of the Boltzmann equation. The calculation proceeds by constructing a series of trajectories, each segment of which is randomly chosen from a distribution of applicable processes. By this method, the values of energy, direction and path length are randomly selected from probability distribution.

Nowadays, more than a dozen program codes used to calculate the transport of electrons, photons, muons, and neutrons through matter are available [22]. Many of these are continuously being improved. Utilizing one of these codes to simulate and optimize the effect of the radiation shielding is the task of another paper [23].

5 Summary

Measuring the irradiation background in the vicinity of the NCP is the principal aim of this work. To this end, a special NaI(Tl) detector is constructed and utilized to measure the γ-ray irradiation continuously. Furthermore, the measurement through dosimeters provide gamma and neutron radiation distributions in the vicinity of the NCP. This is the first time that the radiation distributions near the beam pipe in the storage ring for high energy physics experiments has been obtained. Such information is crucial for the radiation protection design. In fact, compared with previous measurements, it is noticeable that the irradiation background level for the collision mode is much greater than that for the synchrotron mode. Moreover, all measurement results due to IZ-type dosimeters concur in indicating that the neutron radiation level is too high to be safe to locate the HPGe detector at the NCP without any protection.

In the light of the detailed measurement data and model-dependent theoretical estimation, it indicates that rather thick shielding materials, i.e. at least 40 centimeter paraffin or 20 centimeter lead together with 20 centimeter paraffin, are needed to attenuate the fast neutron flux to the acceptable level for the HPGe detector.

6 Note and complement

6.1 Dose-equivalent calculation

This section is devoted to the useful empirical formulas for calculating the removal coefficient. First is the formula for evaluating the microscopic removal cross section of hydrogen [24]

$$\sigma_{\rm r}^{\rm H}(E)[\text{barn}] = 0.9 \cdot \frac{10.97}{E[\text{ MeV}] + 1.66}. \tag{13}$$

In the above formula, and also in the formulas that follow, the content in the square brackets denotes the unit for the corresponding variable.

Secondly, for the element i with atomic mass (denoted by M_i [g·mol^{-1}]) greater than 12 g·mol^{-1}, the microscopic removal cross section is evaluated by formula [24]

$$\sigma_{\rm r}^{i} \equiv \sigma_{\rm r}(M_i)[\text{barn}] = 0.011\ M_i^{2/3} + 0.56\ M_i^{1/3} - 0.35. \tag{14}$$

Thirdly, the relation between the removal coefficient and the microscopic removal cross section for element i is as follows,

$$\mu_{\rm r}^{i} = N^i \cdot \sigma_{\rm r}^{i} = \frac{N_{\rm A} \cdot \rho^i}{M^i} \cdot \sigma_r^i, \tag{15}$$

where $N_{\rm A} = 6.022 \times 10^{23}$ mol^{-1} is the Avogadro constant; ρ^i and M^i are the density and atomic mass of element i, respectively; and N^i is the atom density of element i. For the compound,

$$\mu_{\rm r} = N_{\rm A} \cdot \rho \cdot \sum_j \frac{Q_j^i \cdot \sigma_{{\rm r},j}^i}{M_j^i}, \tag{16}$$

Table 6. Measured and calculated (denoted by superscript "th") microscopic removal cross sections and removal coefficients for various elements and compounds. The measured data are taken from Refs. [21, 25]. The values with $*$ are for compounds instead of elements.

material	symbol	atomic mass/ ($g\cdot mol^{-1}$)	density/ ($g\cdot cm^{-3}$)	σ_r/ (b/atm)	μ_r/ cm^{-1}	σ_r^{th}/ (b/atm)	μ_r^{th}/ cm^{-1}
boron	B	10.811	2.535	0.97±0.10	0.146	0.942	0.133
carbon	C	12.001	1.670	0.81±0.05	0.084	0.990	0.083
aluminum	Al	26.982	2.699	1.31±0.05	0.079	1.429	0.086
iron	Fe	55.847	7.865	1.98±0.08	0.156	1.951	0.165
lead	Pb	207.2	11.347	3.53±0.30	0.118	3.349	0.110
paraffin	$C_{30}H_{62}$	422.5*	0.9*	80.5±5.2	0.118	88.03	0.113

Table 7. Coordinate uncertainties. If two measured coordinates before and after each measurement are denoted as A and B, where A and B can be x, y, or z, then the numbers given in the table are presented by formula $(A+B)/2\pm|A-B|$.

order	first time	second time	third time
①	$(-8.2\pm1.5, 381.0\pm2.0, 120.8\pm1.5)$	$(-4.0\pm0.0, 378.5\pm1.0, 120.8\pm0.5)$	$(-7.2\pm0.5, 381.5\pm1.0, 120.2\pm0.5)$
①a	$(-8.2\pm1.5, 381.0\pm2.0, 170.8\pm1.5)$		
①b	$(-8.2\pm1.5, 381.0\pm2.0, 72.5\pm1.0)$	$(-6.5\pm1.0, 379.0\pm0.0, 71.5\pm1.0)$	
①c	$(-8.2\pm1.5, 381.0\pm2.0, 22.5\pm1.0)$		$(-7.2\pm0.5, 380.5\pm1.0, 20.0\pm1.0)$
②	$(52.4\pm1.2, 371.4\pm0.8, 119.4\pm0.1)$	$(50.5\pm1.0, 373.0\pm2.0, 120.5\pm1.0)$	$(54.0\pm2.0, 370.5\pm1.0, 119.8\pm0.5)$
②a		$(50.5\pm1.0, 373.0\pm2.0, 170.2\pm0.5)$	
②b	$(52.4\pm1.2, 371.4\pm0.8, 68.0\pm2.0)$	$(50.5\pm1.0, 373.0\pm2.0, 69.5\pm1.0)$	
②c		$(50.5\pm1.0, 371.5\pm5.0, 22.8\pm0.5)$	
③	$(-4.2\pm1.5, 423.1\pm1.4, 120.1\pm0.2)$	$(-6.5\pm3.0, 422.5\pm1.0, 120.0\pm0.0)$	$(-2.2\pm0.5, 424.0\pm0.0, 119.8\pm0.5)$
④	$(-49.5\pm1.9, 370.5\pm1.0, 120.2\pm0.2)$	$(-48.5\pm1.0, 372.0\pm1.0, 121.0\pm0.0)$	$(-50.5\pm1.0, 369.0\pm0.0, 119.8\pm1.5)$
⑤	$(-1.5\pm0.0, 320.4\pm1.8, 119.9\pm1.0)$	$(-2.0\pm0.0, 319.8\pm0.5, 119.0\pm0.0)$	$(-1.8\pm0.5, 319.8\pm1.5, 119.8\pm0.5)$
⑥	$(100.1\pm0.2, 369.6\pm0.3, 118.0\pm0.0)$	$(101.0\pm2.0, 370.0\pm0.0, 119.0\pm0.0)$	$(102.2\pm0.5, 371.2\pm0.5, 117.0\pm0.0)$
⑥a			$(102.2\pm0.5, 371.8\pm0.5, 169.0\pm2.0)$
⑥b			$(102.2\pm0.5, 370.8\pm1.5, 70.2\pm0.5)$
⑦		$(150.5\pm1.0, 372.5\pm1.0, 121.0\pm0.0)$	$(147.8\pm2.5, 370.5\pm1.0, 118.5\pm1.0)$
⑧			$(199.5\pm1.0, 372.0\pm0.0, 119.0\pm2.0)$
⑨	$(-100.6\pm0.4, 369.9\pm0.2, 119.8\pm0.3)$		
⑩	$(0.0\pm0.0, 11.5\pm1.0, 119.0\pm0.0)$	$(-2.5\pm1.0, 15.5\pm1.0, 121.0\pm2.0)$	$(2.2\pm0.5, 11.5\pm0.0, 121.5\pm1.0)$
⑩a	$(0.0\pm0.0, 10.0\pm0.0, 20.0\pm0.0)$	$(2.0\pm0.0, 13.0\pm4.0, 20.5\pm1.0)$	$(2.2\pm0.5, 10.8\pm0.5, 18.5\pm3.0)$
⑪	$(-99.5\pm1.0, 1.6\pm0.7, 120.6\pm1.2)$	$(-99.2\pm0.5, 1.0\pm2.0, 121.2\pm0.5)$	$(-99.8\pm0.5, 1.8\pm0.5, 121.2\pm0.5)$
⑫	$(-99.8\pm0.5, -56.6\pm0.0, 123.5\pm1.8)$	$(-99.5\pm1.0, -57.5\pm0.0, 121.2\pm0.3)$	$(-99.0\pm0.0, -56.3\pm0.0, 122.9\pm0.0)$
⑬	$(-98.0\pm0.0, -222.9\pm0.0, 123.8\pm4.3)$	$(-103.2\pm6.3, -223.4\pm0.0, 121.6\pm2.1)$	$(-101.4\pm3.2, -221.3\pm2.0, 114.4\pm9.9)$
⑭	$(-700.0\pm0.0, -56.6\pm0.0, 124.8\pm0.5)$		
⑮		$(-600.0\pm0.1, 57.5\pm0.0, 119.6\pm0.0)$	
⑯			$(-493.5\pm1.0, -56.3\pm0.0, 121.9\pm4.1)$
⑰	$(100.0\pm0.0, 1.8\pm0.4, 122.5\pm5.0)$		
⑱	$(99.0\pm2.0, -60.0\pm0.0, 123.4\pm4.7)$		
⑲		$(300.0\pm0.0, 0.0\pm0.0, 121.0\pm2.0)$	
⑳		$(299.8\pm0.5, 61.5\pm0.0, 118.1\pm0.4)$	
㉑			$(400.2\pm0.5, 0.5\pm0.0, 122.5\pm0.0)$
㉒			$(399.0\pm2.0, -60.0\pm0.0, 117.8\pm0.5)$

where ρ is the density of the compound; Q^i is the weight percent of element i in the compound.

For various elements, the removal coefficients are calculated by formula (15), while for compound (paraffin), the removal coefficient is calculated by formula (16). All calculated results are listed in Table 6, where the measured values are also shown. The comparison between the measured and calculated values indicates that the consistency is fairly good.

6.2 Dosimeter position uncertainty

The coordinates presented in Table 2 should be called designed coordinates, which are the coordinates we plan to locate the dosimeters. But in the actual measurement, such positions cannot be achieved ideally as we designed, since some uncertainties exist due to many practical factors. Therefore, before and after each measurement, the actual coordinates are

measured by the rule with minimum unity of a millimeter. Then the mathematics average of two measured coordinates is used as the position for the certain point and their difference is used as the uncertainty. The data for the measurements of the first three times are presented in Table 7, while those for the fourth time have already been given in the second column of Table 3.

Generally speaking, the uncertainties involving the measurements depicted in this paper are not very small. Besides the coordinate uncertainties listed above, the measurement uncertainties in Table 2 and Table 3 for the gamma and neutron radiation doses are around 15%, according to the information from Landauer [17].

References

1 FU Cheng-Dong, MO Xiao-Hu. Chin. Phys. C (HEP & NP), 2008, **32**: 776–780
2 Design Report of Accelerator BEPC Ⅱ (Accelerator Part) (May, 2002); also could be obtained through web page: http://acc-center.ihep.ac.cn/download/pdr_download.htm
3 Achasov M N et al. The Beam Energy Calibration System for BEPC Ⅱ Collider, arXiv:0804.0159 [physics.acc-ph]
4 MO Xiao-Hu et al. Chin. Phys. C (HEP & NP), 2009, **33**: 914–921
5 MO Xiao-Hu et al. Chin. Phys. C (HEP & NP), 2008, **32**: 995–1002
6 Hsu I C, Chu C C, Yu C I. Phys. Rev. E, 1996, **54**: 5657
7 Ohgaki H et al. Nucl. Instrum. Methdods A, 2000, **455**: 54–59
8 ZHANG Jian-Yong et al. Effect due to Pu-C Source on HPGe Detector and Corresponding Neutron Shielding, Chin. Phys. C (HEP & NP), to be published
9 Knoll G G. Radiation Detector and Measurement. New York: Juhn Wiley & Sons, 1979
10 MAESTRO-32 Software User's Manual (Version 6, 2003, Printed in U.S.A)
11 Physics Analysis Workstation: An Introductory Tutorial (1995, Geneva, Switzerland)
12 Mariscotti M A. Nucl. Instrum. Methods, 1967, **50**: 309–320
13 McKeever S W S. Nucl. Instrum. Methods B, 2001, **184**: 29–54
14 Amgaron K. Long-Term Measurements of Indoor Radon and Its Progeny in the Presence of Thoron Using Nuclear Track Detectors: a Novel Approach, Ph.D. thesis (April, 2002)
15 Durrani S A, Bull R K. Solid State Nuclear Track Detection. New York: Pergamon Press, 1987
16 Fleischer R L, Price P B, Walker R M. Nuclear Tracks in solids: Principles and Applications. Berkely: University of California Press, 1975
17 The Detailed and Comprehensive Introduction about Inlight Dosimeters could be Found Through Web Page: http:// www.landauerinc.com/
18 Leo W R. Techniques for Nuclear and Particle Physics Experiments. Berlin: Springer-Verlag, 1994
19 Martin J E. Physics for Radiation Protection. New York: John Wiley & Sons, 2000
20 Raudorf T W et al. IEEE Trans. on Nucl. Sci., 1984, **NS-31**(1): 253
21 Shultis J K, Faw R E. Radiation Shielding. Illinos: American Nuclear Society & Society, 2000
22 National Council on Radiation Protection and Measurements. Radiation Protection for Particle Accelerator Facilities (NCRP Report No. 144). Bethesda, Maryland: National Council on Radiation Protection and Measurements. 2005
23 WU Qing-Biao et al. Simulation Study of Radiation Fields at the North Crossing Point of BEPC Ⅱ for Energy Eeasurement System, a paper in preparation
24 LI Xing-Hong et al. Elementary of Radiation Protection. Beijing: Atomic Energy Press. 1982 (in Chinese)
25 WANG Ming-Qian, LI Yu-Xiong. Radiation Protection. Hefei: University of Science and Technology of China. 1990 (in Chinese)